ANALYSIS OF ANECHOIC CHAMBER TESTING OF THE HURRICANE IMAGING RADIOMETER

David Fenigstein[1], Chris Ruf[1], Mark James[2], David Simmons[2], Timothy Miller[2], Courtney Buckley[2]

[1]University of Michigan
2455 Hayward St.
Ann Arbor, MI 48109-2143
dfenig@umich.edu

[2] NASA/Marshall Space Flight Center
320 Sparkman Drive
Huntsville, AL 35805

1. INTRODUCTION

The Hurricane Imaging Radiometer System (HIRAD) is a passive microwave synthetic thinned aperture radiometer that operates at the C-Band frequencies 4, 5, 6 and 6.6 GHz. HIRAD was developed for the purpose of observing wind speed and rain rate in tropical cyclones from aircraft over a wider swath than was possible using available technology. Accurate characterization of aperture synthesis radiometers requires the measurement in an anechoic chamber of antenna-pair interference patterns. This paper describes the procedures and analysis of HIRAD anechoic chamber tests made in October 2009, to verify proper measurement of the antenna-pair interference patterns and to develop an image reconstruction algorithm.

2. INSTRUMENT DESIGN

The HIRAD array antenna is composed of linear arrays of stacked multi-resonant radiators, operating at 4, 5, 6, and 6.6 GHz [1,2]. The optimal configuration for 10 1-D antenna elements assigns 36 non-redundant baselines [3]. The elements are spaced at integer multiples of 0.90 inches, resulting in baselines at spacings given in Table I. Each antenna element is connected to a receiver that filters, amplifies and demodulates the signal. The signal is down-converted to an IF frequency and digitized, then introduced to a complex correlator, where each signal is decomposed into in-phase (real) and quadrature-phase (imaginary) parts. The signals are then split into 16 subbands. Complex correlations for all possible pairings of the 10 receivers (45 total) are calculated using complex multipliers at common subbands, giving a measurement of the raw visibility samples [2]. Calibration of the samples is

achieved through hot and cold calibration loads internal to each receiver, and a correlated noise diode[2]. This configuration is depicted in the block diagram in Fig. 1.

TABLE I:

HIRAD DESIGN PARAMETERS

Freq. (GHz)	4.0,	5.0	6.0	6.6
Antenna spacings (in units of λ)	.305	.381	.457	.503
IF Bandwidth	75 MHz			
IF Subbands	16			
# Array Elements	10			
# Antenna Pairs	45			
# Unique Baselines	36			
Sampling Frequency	150 MS/s			

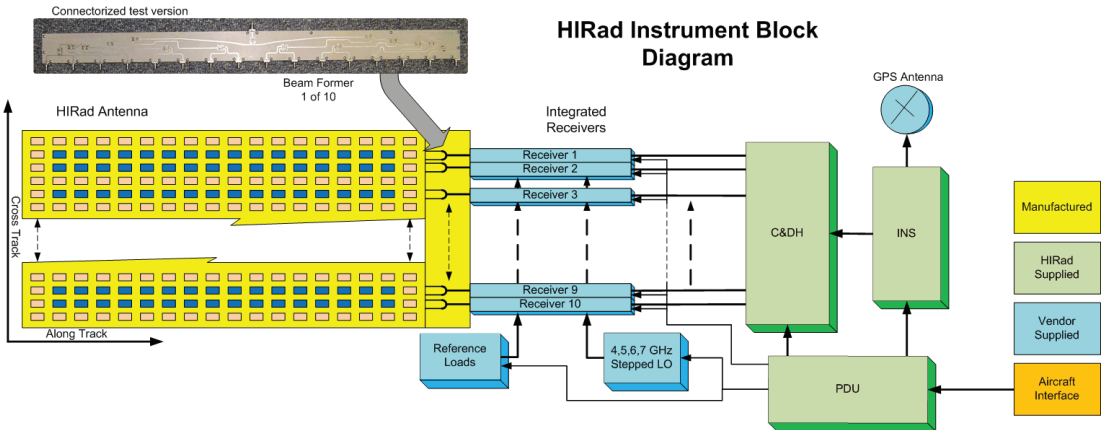

Figure 1: Radiometer System Block Diagram

3. ANECHOIC CHAMBER TEST PROCEDURE

Tests to measure the element patterns, and the cross-track and along-track interference patterns, in the HIRAD system were conducted in an anechoic chamber using a broadband noise diode as a transmitting source. In addition, these scans were repeated with the array rotated 90^0 in order to get a measurement of both the co-pol and cross-pol patterns. The scans were also done with the noise diode off, and these background readings were subtracted from the scans with the source on to remove chamber wall contributions.

The test data underwent initial performance testing to verify that each baseline was producing visibility samples with the expected spatial frequency response. The principal plane cross-scan produces interference patterns as the cross-correlation of each antenna pair according to the relation

$$real\left(S_1 \times S_2^*\right) = \cos^2\left(\theta\right) \times \cos\left(2\pi D_x x\right) \tag{1}$$

where

$$x = \sin\left(\theta\right) \tag{2}$$

$$D_x = n\frac{\lambda}{2}, \quad \lambda = 0,1,2...36 \tag{3}$$

and the complex cross-correlation is computed as [2,4,5]

$$S_1 \times S_2^* = \left(I_1 I_2 + Q_1 Q_2\right) + j\left(I_2 Q_1 - I_1 Q_2\right) . \tag{4}$$

Due to this relation, the Fourier transform of the interference patterns has a peak at D_x, the physical distance between the antennas, and this can be used to verify that the cross-correlations are producing interference patterns at the desired spatial frequencies.

The plots in Figs. 2 and 3 illustrate an example of this relation for one HIRAD baseline of across all four frequency channels. The cross-correlations of antenna elements 8 and 9 (which have a spacing of *n=5)*, can be seen in Fig. 2, with the power spectra in Fig. 3. The abscissa in Fig. 3 represents *n* of equation (3). The peaks in these graphs are at approximately and *n=5,* as expected. Also noticeable in the figures are additional power contributions outside of the peak from the other antennas (near 34). These complex contributions are all factored into the G-reconstruction [4,5].

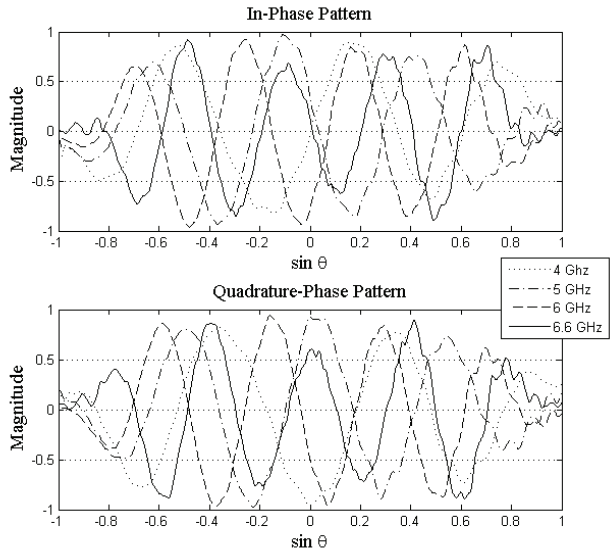

Figure 3: Interference Patterns for antenna pair with baselines 5*λ/2

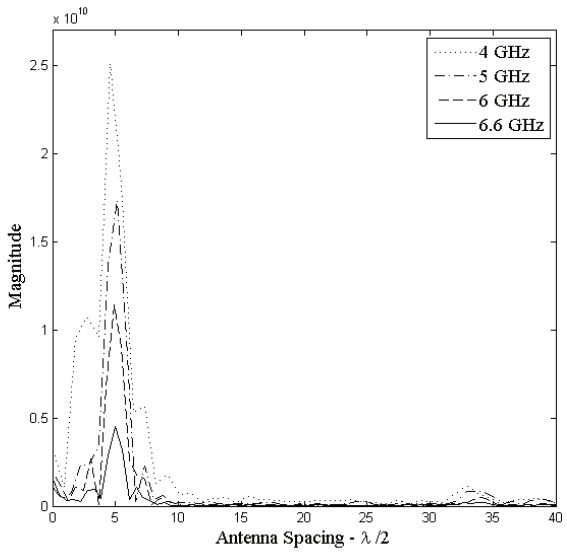

Figure 4: Power spectra for antenna pairs with baselines 5*λ/2

4. SUMMARY

From the anechoic chamber tests, the full complement of visibility samples is available to populate the G-Matrix. The interference patterns for the 45 antenna pairs each produce a peak spatial frequency of the physical spacing between them. By inverting the G-Matrix the image reconstruction formula will be constructed.

5. REFERENCES

[1] C.Ruf, R. Amarin, M.C. Bailey, B. Lim, R. Hood, M. James, J. Johnson, L. Jones, V. Rohwedder and K. Stephens, "The hurricane imaging radiometer – An octave bandwidth synthetic thinned array radiometer," Proc. IGARSS 2007, Barcelona, 23-27 July 2007.

[2] L. Jones, "An application for: Collaborative R&D initiative for the Gulf of Mexico – Development of hurricane forecasting flight instrument HIRAD," Univ. Central Florida, Tech. Rep., 2009.

[3] C. S. Ruf "Numerical Annealing of Low-Redundacy Linear Arrays," *IEEE Trans. Ant. And Prop*, vol. 41, pp. 85–90, Jan.1993.

[4] C. S. Ruf, C. T. Swift, A. B. Tanner and D. M. Le Vine, "Interferometric Synthetic Aperture Microwave Radiometry for the Remote Sensing of the Earth," *IEEE Trans. Geosci. Remote Sens.*, vol. 26, no. 5, pp. 597-611, Sep. 1988.

[5] A. B. Tanner and C. T. Swift, "Calibration of a Synthetic Aperture Radiometer," *IEEE Trans. Geosci. Remote Sens.*, vol. 31, no. 1, pp. 257-267, Jan. 1993.